Published in final edited form as:
Biochemistry. 2012 October 2; 51(39): 7740–7754. doi:10.1021/bi301006w.

Sulfiredoxin redox-sensitive interaction with S100A4 and non-muscle myosin IIA regulates cancer cell motility

Robert R. Bowers[1], **Yefim Manevich**[1], **Danyelle M. Townsend**[2], and **Kenneth D. Tew**[1,*]

[1]Department of Cell and Molecular Pharmacology and Experimental Therapeutics, Medical University of South Carolina, Charleston, SC, USA

[2]Department of Pharmaceutical and Biomedical Sciences, Medical University of South Carolina, 173 Ashley Ave, Charleston, S.C. 29425, USA

Abstract

Sulfiredoxin (Srx) is a redox active protein that participates in the reduction of oxidized cysteine residues. Here we identify a novel function of Srx through its specific binding to S-glutathionylated S100A4 affecting its interaction with non-muscle myosin (NMIIA), thereby modulating the effect of S100A4 on NMIIA function and impacting cell adhesion and migration. Srx forms a complex with S100A4 (and has stronger affinity for S-glutathionylated S100A4), regulates its activity and mediates redox-regulation of the interaction of S100A4 with NMIIA. The consequence of this regulation is microfilament remodeling and altered cellular motility and adhesion. Srx over-expressing cells had reduced adhesion, decreased levels of Tyr^{397}-phosphorylated focal adhesion kinase and increased cell motility in wound healing assays. These results describe a novel redox-sensitive role for Srx in mediating complex protein interactions with plausible consequences to cancer cell motility.

Redox homeostasis is critical for normal physiology and excessive reactive oxygen species are associated with a number of human diseases including cancer. Thiol groups in cysteines are among the most reactive amino acid side chains and are subject to oxidative post-translational modifications such as disulfide bond (S–S), sulfenic (–SOH), sulfinic (SO_2H) and sulfonic (SO_3H) acids and S-nitrosylation (–SNO). In addition, mixed disulfides of protein thiols and glutathione can result from the S-glutathionylation (PS–SG) of low pK_a cysteine residues in certain target proteins. These oxidative cysteine modifications alter the structure and function of a variety of proteins and are involved in cell signaling (1). Sulfiredoxin (Srx) is a ubiquitous antioxidant protein with tissue specific expression patterns and elevated levels in a number of human cancers (2). Initial indications are that Srx1 null mice have no obvious phenotype other than increased sensitivity to lipopolysaccharide-induced endotoxic shock (3) and increased sensitivity to ethanol-induced oxidative toxicity in liver (4). Srx was originally identified as a Mg^{2+} ATP-dependent sulfinic acid reductase specific to 2-Cys peroxiredoxins (Prxs), where it catalyzes reactivation of hyper-oxidized (sulfinic acid) Prxs (5–7), but a few studies have shown that Srx possesses deglutathionylating activity towards actin, PTP1B and PrxI (5, 8, 9).

Even in the absence of precise mechanism(s), Srx expression has been linked with both cell division and tumorigenicity (2, 9). In the present study, we sought to address this connection by identifying binding partners of Srx. We identified several novel candidate proteins that

*Corresponding author: Dr. Tew K.D., Department of Cell and Molecular Pharmacology and Experimental Therapeutics, Medical University of South Carolina, Charleston, SC, USA. Phone: 843 792 2514; Fax: 843 792 9588; tewk@musc.edu.

The authors declare no competing financial interests.

co-immunoprecipitated with Srx. Among these the heavy chain of non-muscle myosin IIA (NMIIA) is in a position downstream of convergent signaling pathways central to cell adhesion, migration and microfilament architecture (10). In addition, Srx was also found to co-immunoprecipitate with S100A4 - a calcium binding protein that plays a key role in regulating NMIIA activity (11). These observations led us to consider whether Srx may be involved in some aspect of regulation of cell migration. Cell migration is typically viewed as a series of coordinated steps. Initially, either broad (lamellipodia) or spike-like (filopodia) protrusions of the membrane, or both, extend in the direction of migration. These membrane extensions are driven by polymerization of actin filaments and stabilized by nascent cell adhesions that link the underlying extracellular matrix to the actin cytoskeleton. Actomyosin based contractions provide the force necessary to generate traction and to initiate detachment of adhesions at the rear of the cell. Rho family GTPases and their targets, especially tyrosine kinases, regulate the dynamics of focal complexes and actomyosin filaments (12). Moreover, ROS and redox conditions influence the actomyosin complex. For example, NOX family enzymes are linked to invasion and metastasis (13, 14). NOX generated superoxide anion radicals can spontaneously dismutate into H_2O_2 facilitating interaction with NO (with $NOOO^-$ generation) and subsequent nitrosation of protein cysteines. In the presence of the high levels of GSH in the cytosol (2–10mM) S-nitrosylated cysteines can be rapidly converted to S-glutathionylated residues and these directly influence actin-myosin interactions and the polymerization state of actin (15–17). Srx may participate in deglutathionylation of actin (8) providing a redox-mediated mechanism for regulating actin polymerization.

There are over twenty S100 proteins in the human genome. They are low molecular weight proteins with conserved structural motifs of two EF-hand Ca^{2+}-binding domains connected by a variable hinge region (18). Specific S100s can regulate calcium homeostasis, cytoskeletal rearrangements, cell proliferation and apoptosis. Calcium binding causing S100 structural rearrangements can expose hydrophobic residues and result in Ca^{2+}-dependent interactions with target proteins (19). Cysteine residues within S100 homologues are highly conserved between species and are subject to S-glutathionylation (20–22). S100A4 is a metastasis associated Ca^{2+}-binding protein found in aggressive tumors that interacts with the tail region of NMIIA preventing filament formation and promoting the disassembly of filaments resulting in enhanced cell migration (23, 24). Recent reports identify a critical role for Cys residue 81 of S100A4 in regulating its interaction with NMIIA (25).

In the present study we identified S100A4 and NMIIA as part of a protein complex with Srx. *In vitro* FRET-based analyses demonstrated tight binding (low nanomolar K_D) of Srx and S100A4. Further, the catalytic Cys of Srx was shown to be involved in this binding and S-glutathionylation of S100A4 markedly increased the Srx:S100A4 interaction, observations consistent with redox regulation of the Srx:S100A4 interaction. Oxidative stress increased the interaction of Srx with both NMIIA and S100A4. In addition, we found that Srx expression levels have a marked affect on cell adhesion, actin microfilament architecture, and cell migration, likely as a consequence of Srx-mediated redox-regulation of S100A4 – NMIIA interactions. There are implications for these data that involve Srx and this protein complex in cancer cell migration and metastasis.

Experimental Procedures

Reagents

General chemicals and FLAG® immunoprecipitation kits were from Sigma (St Louis, MO). Dulbecco's Modified Eagle Medium (DMEM)/Ham's F12 50/50 mix was obtained from Mediatech Inc. (Manassas, VA). A monoclonal antibody against human sulfiredoxin was produced in the MUSC core facility as described (9). The monoclonal antibody against S-

glutathionylated protein was purchased from Virogen (Watertown, MA). Rabbit polyclonal antibodies to non-muscle myosin IIA (ab24762) and S100A4 (ab41532) were from Abcam (Cambridge, MA). Rabbit polyclonal antibodies against focal adhesion kinase (FAK; #3285) and phospho-FAK (#3283) were from Cell Signaling Technology (Danvers, MA). Rhodamine Red™-X-conjugated donkey antirabbit and horseradish peroxidase-conjugated donkey anti-rabbit and anti- mouse secondary antibodies were from Jackson ImmunoResearch (Westgrove, PA). CNBr-activated sepharose was obtained from GE Healthcare (Piscataway, NJ). Oregon Green® 488 phalloidin and Prolong® Gold antifade reagent with DAPI was from Invitrogen (Carlsbad, CA). Alexa®546 N-succinimidyl ester and QSY®35 acetic acid, succinimidyl ester was from Invitrogen (Carlsbad, CA). PABA/NO was provided by Dr. Larry Keefer, NCI, Frederick, MD. (26). Recombinant human S100A4 protein was from R&D Systems (Minneapolis, MN). Lab-Tek™II Chamber Slides™ were obtained from Nalge Nunc International (Rochester, NY).

Cell culture

Non-small cell lung cancer derived A549 cells (American Type Culture Collection; Manassas, VA) were maintained in DMEM/F12 50/50 containing 10% fetal bovine serum (FBS). A549 cells expressing FLAG-tagged Srx were as described previously (9). Knockdown of sulfiredoxin expression by shRNA retroviral gene transfer was accomplished using the pLK01.1 vector and 1.2mg/ml puromycin selection according to the protocol of the manufacturer (Clontech Laboratories, Inc.; Mountain View, CA). Nitrosative stress in WT, KD and OE A549 cells was induced by an addition of PABA/NO (20 μM) to cell monolayers in complete media. After 20 min incubation at 37°C, cells were washed three times with ice-cold PBS and lysed with Triton lysis buffer (27). The supernatants of control and treated cell lysates (14,000g, 10 min) were used for protein concentration analyses (Bradford) and electrophoretic resolution of the proteins by SDS PAGE.

Immunoblot and immunoprecipitation

Cells were washed with cold phosphate buffered saline (PBS) and lysed in Triton lysis buffer. Immunoprecipitation of FLAG-tagged Srx was achieved using FLAG® immunoprecipitation kit according to the protocol of the manufacturer (Sigma; St Louis, MO). For immunoprecipitation of NMIIA, primary antibodies were conjugated to cyanogen bromide-activated Sepharose according to the manufacturer's recommendations (GE Healthcare; Piscataway, NJ). Cell lysates (~1mg of total protein) were incubated with a sepharose-conjugated antibody overnight at 4°C under constant agitation. The sepharose immunoprecipitate was separated by centrifugation (14,000 g, 5 min). After washing 3 times with PBS, the precipitated proteins were separated from the sepharose-conjugated antibody by acidification with glycine buffer (0.5M, pH 2.1 containing 150 mM NaCl) and collected by centrifugation (14.0×10^3 g, 15 min, 4°C). Cell lysates and immunoprecipitates were resolved by 12% SDS-polyacrylamide gel electrophoresis and transferred onto PVDF membranes (Bio-Rad; Hercules, CA). Nonspecific binding was blocked by incubating membranes in TBST (Tris-buffered saline with 0.1% Tween-20) containing 5% non-fat dry milk or 5% bovine serum albumin Fraction V. Primary antibodies were incubated for two hours at room temperature or at 4 °C overnight and secondary HRP-conjugated antibodies were incubated for one to two hours at room temperature. The blots were developed with ECL (GE Healthcare Bio-Sciences Corp.). The blots were scanned with a BioRad ChemiDoc system and visualized with a trans-illuminator.

Liquid chromatography coupled to electrospray ionization tandem mass spectrometry

Immunoprecipated samples were treated with 9 volumes of cold acetone. The pellet was then re-dissolved with Rapigest (Waters; Milford Massachusetts) and the manufacturer's protocol was followed for trypsin digestion. Trypsin digested samples were analyzed via

liquid chromatography (LC)-electrospray ionization (ESI) -tandem mass spectrometry (MS/MS) on a linear ion trap mass spectrometer (LTQ, Thermo Finnigan) coupled to an LC Packings nano LC system. A C-18 reversed phase LC column (packed in house, 15cm, 75 μm inner diameter, particle size 5μm) was used eluted with linear a 60 minute gradient from 2% acetonitrile, 0.1% formic acid to 60% acetonitrile, 0.1% formic acid. A blank injection was analyzed between samples to limit carry over. Data Dependent Analysis was utilized on the LTQ to perform MS/MS on the 10 most intense ions in each MS spectra with a minimum ion count of 1000. Dynamic Exclusion was set to exclude ions from MS/MS selection for 3 minutes after being selected 2 times in a 30 second window. The MS/MS data were searched against the human database (http://www.ncbi.nlm.nih.gov/protein) utilizing Thermo Finnigan Bioworks 3.3.1 SP1 software. Variable modifications of methionine oxidation, carboxamidomethylation of cysteines, and phosphorylation of serine, threonine, and tyrosine were considered. Protein identifications must meet the minimum criteria of a Protein Probability of 1.0 E^{-3} or better and have an Xcorr vs charge state > 1.5, 2.0, 2.5 for +1, +2, and +3 ions, with at least 2 unique peptides matching the protein, and a good match for at least 4 consecutive y or b ion series from the MS/MS spectra.

Molecular modeling of Srx interaction with S100A4

Modeling of binary protein interactions was performed using ZDOCK software (http://zdock.bu.edu) without any restriction to individual protein structural elements or sequences. Only models with the highest probability score were selected for further analysis. The crystal structure of human Srx (PDB, 1XW3, in complex with ADP) and S100A4 (PDB, 3CGA) were used for modeling. Individual protein structure and binary models were visualized using RasMol (V2.7.5, http://www.bernstein-plussons.com/software/rasmol/doc/rasmol.html) software.

Sulfiredoxin interaction with S100A4

Purified Srx (C99S) protein was incubated with 5x excess of succinimidyl ester of Alexa®546 Fluor carboxylic acid (Invitrogen) and S100A4 (S100A4-SSG) purified protein was incubated with 5x excess of succinimidyl ester of QSY®35 acetic acid (Invitrogen) at room temperature, overnight, under constant agitation to label primary amines according to manufacturer's recommendations. The reaction mixture was processed using a BioSpin 6 (BioRad) size-exclusion spin column to remove an excess of unreacted dyes and exchange reaction buffers to 20mM PB (pH 7.4). Spectroscopic analysis of Alexa®546 Fluor label incorporation indicated ~2.0 mol of dye per 1 mol of Srx or C99S mutant monomer. *In vitro* S-glutathionylation of S100A4 (25μg in 1.0 ml of 10mM PB, pH=7.4) was performed with 50μM PABA/NO and 1mM GSH (room temperature, 1hr, under constant stirring) using procedures previously described (28). We designed the HPLC analysis, which allowed monitoring all reactants simultaneously. HPLC was performed with Binary HPLC Pumps 1525 separation unit, Dual λ Absorbance Detector 2487, and 717plus Autosampler (all from Waters, Milford, MA). We used C_{18} column 4.6×150 mm, 5 μm particles size, and 100Å pore size (SunFire, Waters, MA) and isocratic elution (1 ml/min) with [(H_2O +0.1% TFA): (ACN + 0.1% TFA) = 45:55 (V:V)] mixture and detection at 220 nm. The chromatography and data processing were performed using Empower™ 2 Chromatography software (Waters, Milford, MA). The data are representive of three independent experiments.

The reaction mixture was processed using a BioSpin 6 size-exclusion micro-column to eliminate excess reagents and resulted in essentially homogeneous (>98% purity) S-glutathinylated S100A4. Resultant S-glutathionylated proteins were detected by western blot with anti-glutathionylated antibodies (Virogen, Watertown, MA). Intact and S-glutathionylated S100A4 were used for fluorescent labeling with succinimidyl ester of

QSY®35 acetic acid. Spectroscopic analysis of QSY®35 label incorporation showed ~3.0 mol of dye per 1 mol of S100A4 or S100A4-SSG protein monomers.

Concentrations of all proteins were determined spectroscopically: Srx and C99S mutant using ε= 7280 $M^{-1}cm^{-1}$ at 280 nm (29); Alexa®546 – labeled Srx (C99S) using a correction coefficient of 0.12 for the label absorbance (ε= 104000 $M^{-1}cm^{-1}$ at 554 nm) at 280 nm; S100A4 (S100A4-SSG) using ε= 3040 $M^{-1}cm^{-1}$ (23) at 280 nm; and S100A4 (S100A4-SSG) labeled with QSY®35 using a correction coefficient 0.23 for the label absorbance (ε= 24000 $M^{-1}cm^{-1}$ at 490 nm) at 280 nm.

The fluorescent analysis of the FRET-based (R_0=25 Å for Alexa®546/QSY®35 couple) protein binding was performed using the QM-4 spectrofluorometer (PTI, Birmingham, NJ). We used 1.0 or 2.0 nM of Alexa®546-labeled hSrx(C99S) in 10 mM PB, pH=7.4 for our titration experiments. Titration was performed in 5×5×40 mm quartz cuvette in a fluorometer sample holder at room temperature. Emission spectra of both the Alexa546-labeled Srx (C99S) were recorded (Ex.=546 nm) before any additions. Because of higher accuracy of measurements at low concentrations of protein we used integration of the emission spectra as a measure of FRET effect on the “donor” (Alexa®546) fluorescence. The indicated amounts (0.5–400 nM) of QSY®35-labeled S100A4 were added to 2.0 nM of Alexa®546-labeled Srx (C99S) in solution. After incubation for ~5 min under constant shaking to reach equilibrium between “free” and “bound” S100A4, the emission spectra of Alexa®546 with the indicated concentrations of S100A4-QSY®35 were recorded. The effect of each S100A4-QSY®35 concentration was measured individually. To eliminate any variation in actual concentrations of Srx (C99S) any differences between the integration of the latter and the initial Alexa®546 spectra were normalized to the integral of the initial emission spectra. Similarly, the indicated amounts (0.2–250 nM) of S100A4-SSG- QSY®35 were added to 1.0 nM of Alexa®546-labeled Srx (C99S) in solution. All experimental details were the same as for titration with S100A4- QSY®35. The results were corrected for an effect of sample dilution. The Y-axis of graphic representation of experimental data corresponds with the decrease of Alexa®546 emission, which is proportional to amount of S100A4(S100A4-SSG)-QSY®35 bounded to Srx (C99S). The X-axis represents a total amount of added S100A4 or (S100A4-SSG) labeled with QSY®35. Each titration point was performed in triplicate and presented as mean±SD.

The experimental data for S100A4 binding to Srx(C99S) were processed using a “One Site Saturation model” (Pharmacology application, SigmaPlot 10.0, SyStat, MA) with best hyperbolic fit ($R^2 \geq 0.99$) according to equation for one binding site:

$$Y=B_{max1}{}^{*}X/(K_{D1}+X) \quad (1)$$

where: X – is a concentration of added S100A4 protein; Y – is a normalized decrease of Alexa®546 fluorescence corresponding to specific binding of S100A4; B_{max1} – is a saturated number of binding complexes with apparent equilibrium dissociation constant K_{D1}.

The experimental data for S100A4SSG binding to Srx(C99S) were processed using a “Two Site Saturation model” (Pharmacology application, SigmaPlot 10.0, SyStat, MA) with best hyperbolic fit ($R^2 \geq 0.99$) according to the equation for two binding sites with different affinities:

$$Y=B_{max1}{}^{*}X/(K_{D1}+X)+B_{max2}{}^{*}X/(K_{D2}+X) \quad (2)$$

where: X – is a concentration of added S100A4(S100A4SSG) protein; Y – is a normalized decrease of Alexa®546 fluorescence corresponding to specific binding of S100A4; B_{max1} –

is a saturated number of high affinity binding complexes with apparent equilibrium dissociation constant K_{D1}; B_{max2} – is a saturated number of lower affinity binding complexes with apparent equilibrium dissociation constant K_{D2}.

Competition experiments were used to determine what effect (if any) Srx or Srx(C99S) fluorescent labeling had on the specificity of its binding to S100A4. We used 2 nM of Srx or Srx(C99S)-Alexa®546 for these experiments. At each point of titration an emission spectra of Alexa546 were recorded before and after 5 min incubation with an indicated amount of S100A4-QSY®35. Following this, 2.0 nM of unlabeled Srx or Srx(C99S) were added and after 5 min of incubation (RT), the emission spectra of Alexa546 were recorded. In parallel experiments 2.0 nM solution of Srx or Srx(C99S)-Alexa®546 was added 2.0 nM of intact unlabeled protein and emission spectra were recorded. All emission spectra were integrated and used to generate the titration curves according to the formula:

$$E=(\int_{INT}-\int_{S100A4})/\int_{INT,} \quad (3)$$

where: E – is a normalized decrease of Alexa®546 emission caused by the S100A4- QSY35 binding-mediated FRET; $\int_{INT}$ - corresponds to the integration of Alexa546-labeled or unlabeled mixed with intact Srx(C99S) protein emission spectra, and $\int_{S100A4}$ – corresponds to integration of emission spectra of Alexa546-labeled or mixed with intact Srx(C99S) after incubation with the indicated amounts of S100A4-QSY®35. All spectra were corrected for trivial dilution effects.

To determine if S100A4 fluorescent labeling with QSY®35 altered the specificity of its binding to Srx(C99S) we used “back titrations” with intact unlabeled S100A4 protein. After addition of 150.0 nM of S100A4-QSY®35 to 2.0 nM of Srx or Srx(C99S)- Alexa®546 and incubation for 5 min at room temperature the indicated amounts of intact unlabeled S100A4 were added and incubated for additional 5 min at room temperature under constant stirring. The emission spectra of 2.0 nM of Srx- or Srx(C99S)-Alexa®546 before and after incubation with 150.0 nM of S100A4-QSY®35 were recorded. Similarly, the emission spectra of 2.0 nM of Srx- or Srx(C99S)-Alexa®546 after incubation with 150.0 nM of S100A4-QSY®35 and addition of indicated amounts of intact unlabeled S100A4 were recorded. All emission spectra were corrected for trivial dilution effects, integrated and used for generation of “back-titration” curves according to formula:

$$E=(\int_{INT}-\int_{S100A4(SAT+UL)})/\int_{INT,} \quad (4)$$

where: E – is a normalized decrease of Alexa®546 emission caused by the S100A4-QSY35 binding-mediated FRET; $\int_{INT}$ - corresponds to integration of Srx(C99S)- Alexa®546 (2.0 nM) emission spectra, and $\int_{S100A4(SAT+UL)}$ – corresponds to integration of emission spectra after addition of 150 nM of S100A4-QSY®35 and an indicated concentrations of intact unlabeled S100A4.

The results of competition between Alexa®546-labeled and unlabeled intact Srx or Srx(C99S) binding of QSY®35-labeled S100A4 were analyzed using the standard (as above) SigmaPlot pharmacological application, and “One Site Saturation model” (SigmaPlot 10.0). The latter showed the best fit for the experimental data ($R^2 \geq 0.98$). The results of analysis are presented in Fig. 6 (panels A and B) as mean±SD for 3 independent experiments.

To determine what influence, if any, the QSY®35-labeling of S100A4 has on its binding to Srx(C99S) (mean±SD for 3 independent experiments) binding isotherms of the “back-titration” experiments were carried out (Fig. 6 (panel C)). The same experimental data presented as an increase of Alexa546 fluorescence (as a result of decreased quenching) after

titration with increasing amounts of intact S100A4 were used to calculate an intrinsic equilibrium K_D for the Srx or Srx(C99S)-Alexa546-S100A4 complex using hyperbolic fit and a standard SigmaPlot pharmacological application (SigmaPlot 10.0).

CD analysis

100 μM of rhS100A4 was analyzed in 10 mM PB (pH 7.4) before and after S-glutathionylation (1 mM GSH and 50 RM PABA/NO, 1 hr, at room temperature; excess of reagents were removed by BioSpin-6 micro filtration) in 2×10×40 mm quartz cuvettes in a CD spectrometer (AVIV, model 420, Lakewood, NJ) at 22°C in far UV region 180–260 nm with step size 0.5 nm and averaging of two repeats. The effects of Ca^{2+} were evaluated by addition of 150 μM $CaCl_2$ or 2.0 mM EGTA. Actual CD data were recalculated as molecular ellipticity units according to protein concentration and amino acid content. Background of all used reagents was subtracted from final spectra.

Fluorescent imaging of actin microfilaments and focal adhesions

For visualizing actin microfilaments and focal adhesions in spreading cells, 2×10^3 cells were seeded onto 4-well Lab-TekTM II Chamber Slides™ that were previously coated with 10 μg/mL human fibronectin. After allowing the cells to adhere overnight, cells were fixed with 4% paraformaldehyde for 30 minutes. Cells were permeablized by 20 min incubation in 0.2% Triton X-100 in PBS. Non-specific protein binding was blocked by incubating the cells with 1% bovine serum albumin (BSA) in PBS for 20 minutes. Cells were then incubated for 1 hour in the primary anti-phospho-FAK antibody diluted 1:100 in 1% BSA in PBS. After washing away unbound primary antibody with three rinses of PBS containing 0.05% Tween-20, cells were incubated with Rhodamine Red™-X- conjugated secondary antibody and Oregon Green® 488-conjugated phalloidin. Labeled cells were imaged by fluorescent microscopy (Nikon eclipse E800, Nikon Instr., Inc, Lewisville, TX with Nikon DS-U1 software v. 5.03, Photometrics, Tucson, AZ).

Cell adhesion, globular and filamentous actin, and migration assays

For cell adhesion assays, 1×10^5 cells were seeded onto 24-well cell culture dishes that had been coated with 5 μg of fibronectin or heat denatured bovine serum albumin (BSA). After allowing the cells to adhere for 2 hours, cells that had not adhered were removed by gently rinsing the wells with PBS three times. The adherent cells were fixed with 4% paraformaldehyde and stained with crystal violet. The crystal violet was solubilized with 0.1 M acetic acid and the absorbance at 570 nm was read. The number of cells that adhered to BSA was negligible. For determining the ratio of globular (G) to filamentous (F) actin, cells were lysed in buffer containing 1% Triton X-100. Under these conditions, F actin remains insoluble and was separated from G actin by centrifugation at 16,000 g. The pellets containing F actin were re-suspended in Laemmli sample buffer by passing through a 20-gauge needle and sonication. Equal amounts of supernatants and pellets were resolved by SDS PAGE. For wound healing assays, 1×10^6 cells were seeded onto 3.5 cm dishes. The next day cell monolayers were wounded with a 200 μl pipette tip, and 4X images were acquired after 24 hrs. Three independent measurements using ImageJ 1.45 (http://rsbweb.nih.gov/ij/download.html) were used to quantify cell migration.

Statistical analysis of experimental data

All experimental data were statistically evaluated using SigmaStat 3.5 (Systat Software Inc., San Jose, CA) and represented as a mean±SD. ANOVA was used to evaluate the significance of differences between control and treatment groups.

Results

Immunoprecipitation of sulfiredoxin reveals novel binding partners

To identify binding partners of Srx, FLAG-tagged Srx was immunoprecipitated from A549 cells and resultant proteins identified by liquid chromatography (LC)-electrospray ionization (ESI)-tandem mass spectrometry (MS/MS). Lysates from control cells transfected with the empty FLAG-vector were used to control for non-specific binding of proteins to the FLAG-affinity resin. After excluding these proteins, plus keratins and immunoglobulins, eight proteins were identified (Table 1). As expected, Srx itself was detected in the immunoprecipitates from A549 cells expressing FLAG-tagged Srx but not in the vector only controls. Protein tyrosine phosphatase 1B [PTP1B; (9)], PrxIII and PrxIV (6) have been identified earlier as Srx binding partners and their detection validated the reliability of the method. Four proteins not previously reported to interact either directly or indirectly with Srx were identified. Of these, kinesin family member 11 (KIF11or Eg5) is implicated in spindle movement prior to, and during, anaphase (30) and its expression correlates with the response of non-small cell lung cancer to drugs (31). Other reports link the protein with vesicle transport from the Golgi apparatus to the endoplasmic reticulum (32). Silencing of Serine protease 3 (PRSS3) has been suggested as a putative tumor suppressor gene in non-small cell lung cancer (33). Furthermore, serine protease inhibitors are regulated by reversible S-glutathionylation (34) providing a putative connection with Srx mediated regulation of redox status for this complex of protease and protease inhibitor. Calmodulin-like protein 5 binds Ca^{2+} with high affinity (35) and we have found that S-glutathionylation of eNOS (27) is directly linked with increases in Ca^{2+} flux and calmodulin activation. These observations are consistent with the involvement of Srx with Ca^{2+} pathways.

In context with the cell motility studies, the association between Srx and NMIIA heavy chain polypeptide 9 was studied in more detail. Moreover, although in this experiment S100A4 was not identified as an Srx binding partner, it should be noted that the method is not exhaustive and in our present study the Srx:S100A4 interaction was confirmed by *in vitro* FRET-based studies and subsequent co-immunoprecipitation analyses.

Srx interaction with NMIIA and S100A4

To confirm intracellular binding of Srx to NMIIA we repeated the immunoprecipitation of FLAG-tagged Srx from A549 cells and detected NMIIA protein by immunoblotting (Fig. 1A). Lysates from control cells transfected with the empty FLAG-vector were used as control for non-specific binding of proteins to the FLAG-affinity resin. Further, immunoprecipitation of NMIIA from wild type (WT) A549 cells followed by immunoblotting for Srx confirmed the interaction of NMIIA and Srx in A549 cells expressing endogenous Srx, demonstrating the Srx:NMIIA interaction is not an artifact of Srx over-expression (Srx OE; Fig. 1B). Increasing oxidative stress with H_2O_2 increased the amount of Srx that interacted with NMIIA. As a consequence of the marked difference in size between NMIIA (~250 kDa) and Srx (~12 kDa) multiple nonfunctional interactions may occur. Simultaneously, we also detected S100A4 following Srx immunoprecipitation from the Srx OE cells and the amount of Srx interacting with S100A4 also increased following H_2O_2 treatment (Fig. 1C). As a control for non-specific binding, lysates were exposed to sepharose beads coupled to rabbit IgG. Based on studies described below, we determined that the upper bands in the input lanes of Fig. 1C are S-glutathionylated S100A4 dimers, and it appears that the Srx immunoprecipitates primarily contain this post-translationally modified S100A4.

Immunocytochemistry showed that both S100A4 and NMIIA co-localized with Srx in the perinuclear region of A549 cells, providing additional evidence that these proteins interact in

A549 cells (Fig, 2; also note the strong Srx staining around the plasma membrane). These data did not distinguish whether the interaction between Srx and S100A4 is direct or indirect, i.e. as part of the complex with NMIIA. Therefore, *in silico* modeling and *in vitro* studies were performed to interrogate possible direct interactions between Srx and S100A4. Molecular modeling shows a best-fit complex between the Srx and S100A4 homodimer (Fig. 1D). In this model, Srx interacts with a monomer of intact dimeric S100A4 (2Q91, PDB). In this complex the close proximity (~13 Å) of the single catalytic Cys99 of Srx to the conserved Cys86 of S100A4 could provide a redox-sensitive environment for modification of either cysteine and be critical for stability of this complex. Cys81 occurs in the same canonical target binding cleft (α-helix) of the S100A4 monomer and it may also participate in redox-dependent binding with Srx. In addition, covalent modification of Cys81 was previously shown to inhibit S100A4:NMII binding (22). To address Srx binding to S100A4, we studied the Srx-S100A4 interaction *in vitro* using FRET-based analysis of fluorescently labeled proteins. Further, to understand the role of the Srx catalytic Cys99 in its binding to S100A4 we utilized a catalytically inactive C99S mutant of Srx. Our data show reasonable binding affinity for the recombinant human (rh) S100A4 with purified intact Srx (apparent equilibrium K_D~83.0nM). The affinity of rhS100A4 for the inactive Srx C99S mutant was higher (apparent equilibrium K_D~43.0nM), suggesting that the catalytic cysteine of Srx is of consequence to this binding (Fig. 3A). S100A1, S100A4, S100A6, S100A9 are all substrates for S-glutathionylation *in vivo* (20–22). S100A1 is closely related to S100A4 and S-glutathionylation of its Cys85 (homologous to Cys86 of S100A4) increases its Ca^{2+}-binding affinity (20). In addition, the thiol reactive drug NSC 95397 can modify Cys81 and Cys86 of S100A4, where treatment inhibits the interaction between S100A4 and NMIIA (22). Thus, we S-glutathionylated purified rhS100A4 *in vitro* and studied its binding to WT Srx and Srx C99S mutant. The affinity of S-glutathionylated S100A4 for WT Srx was markedly enhanced compared to intact protein and Srx:S100A4 binding became biphasic (apparent equilibrium K_{D1}~4.8 nM, and K_{D2}~131.0 nM), most likely as a consequence of a specific effect of the GSH-moiety on the S100A4 surface. It is plausible that high affinity binding of S100A4-SSG affects Srx structure and results in formation of low affinity binding sites. S-glutathionylation of S100A4 mildly affected its binding to the catalytically inactive Srx C99S mutant (apparent equilibrium K_D~21.0nM), indicating a role for this residue in the Srx-S100A4-SSG complex formation (Fig. 3B and Table 2). Thus, the upper bands in Fig. 1C likely represent S-glutathionylated S100A4 that is preferentially bound by Srx.

Srx influences S-glutathionylation of S100A4

We have previously used NO donors to induce S-glutathionylation of a variety of proteins (28). As anticipated, treatment of A549 cells [control (WT), Srx depleted by shRNA (KD) and Srx over-expressing (OE)] with the NO donor PABA/NO (20 μM, 20 minutes) increased S-glutathionylation of multiple proteins in all cases (Fig. 3C, left panel). The untreated control cells displayed no detectable S-glutathionylation. Re- probing the same blot with anti-S100A4 antibody revealed that the S100A4 dimer was S-glutathionylated – the upper band migrating at ~30 kDa on the S100A4 blot superimposes with the lower band on the PS-SG blot suggesting that the S100A4 dimer is S-glutathionylated. Further, S-glutathionylation of S100A4 is markedly increased in Srx OE cells (Fig. 3C, right panel). Re-probing of the same blot with anti-actin antibody demonstrated similar protein loading in all lanes (Fig. 3C, right panel). These data indicate that Srx directly influences S100A4 homeostasis in A549 cells.

Next we tested the effect of Ca^{2+} on WT and C99S Srx interaction with S100A4 and S-glutathionylated S100A4 (S100A4-SSG). The affinity of S100A4 binding to Srx was increased by Ca^{2+} (Table 2). Ca^{2+} binding to S100A4 is known to affect its conformation

and promote binding to target proteins (36). Circular dichroism (CD) showed that S-glutathionylation had minimal impact upon S100A4 secondary structure (Fig. 4A). In the presence of Ca^{2+} we detected a small decrease of α-helical content of S-glutathionylated S100A4, likely corresponding to a slight increase in protein hydrophobicity (Fig. 4A). The CD spectra of intact S100A4 + Ca^{2+} almost coincides with that of the S100A4-SSG + Ca^{2+} spectra so it is not presented.

Generally, protein tryptophan fluorescence can be used to evaluate tertiary and/or quaternary structural changes. However, since, S100A4 does not have tryptophanyl residues, we used tyrosine fluorescence of rhS100A4 (Fig. 4B) and rhS100A4-SSG (Fig. 4C) to demonstrate that Ca^{2+} decreased fluorescence (Em ~304 nm) of the S100A4 indicating conformational changes that altered tyrosine exposure to the polar environment. For the S-glutathionylated S100A4, Ca^{2+} binding produced a pronounced change in protein tertiary and/or quaternary structure, measured as an increase of the non-ionizable, excited state for tyrosine – tyrosinate at ~345 nm (37). These data indicate effective binding of Ca^{2+} to both intact and S-glutathionylated S100A4 causing alterations in the tertiary (quaternary) structure of the latter. Accordingly, our data show that generally the affinity of Srx for S100A4 (S100A4-SSG) was increased by the presence of Ca^{2+} (Table 2).

S-Glutathionylation of S100A4 in vitro

HPLC analysis of starting material and products of S100A4 S-glutathionylation by the PABA/NO:GSH mixture *in vitro* was conducted to confirm that the S-glutathionylated S100A4 used in the *in vitro* binding studies was homogeneous. HPLC analysis showed completion of reaction in 1.0 h at room temperature (Fig. 5). The reaction mixture contained 2 nmol of S100A4, 2.5 nmol of PABA/NO, and 50.0 nmol GSH in 1.0ml of 10mM PB, pH=7.4. The starting intact S100A4 was undetected in the reaction mixture after 1.0 h. After 1.0 hr incubation, PABA/NO and GSH concentrations were decreased by 62 and 80% respectively. Retention time (RT) for intact PABA/NO was ~5.25 min and increased after 1.0 h of reaction to ~5.35 min. RT for intact S100A4 was ~10 min and increased after 1.0 h of incubation to 10.5 min. RT for GSH (~8.65 min) was not affected by the reaction. SEC of reaction products with micro bio-spin 6 columns (BioRad) resulted in isolation of >98% chromatographically homogeneous S-glutathionylated S100A4. This material, together with intact S100A4 protein, was used for titration of Srx and C99S. PABA/NO has a strong absorbance peak at ~215 nm and it increased by ~50% after 1.0h reaction with GSH (27). Thus, the decrease of the PABA/NO peak is indicative of its reaction with GSH and S100A4 protein.

Our control experiments show that the affinity of S100A4 binding to Srx or Srx(C99S) was essentially unaffected by labeling of the latter with Alexa®546. The apparent equilibrium dissociation constants for labeled Srx (K_D ~61 nM) or Srx(C99S) (K_D ~ 30 nM) were similar to those where unlabeled intact Srx (K_D ~60 nM) or Srx(C99S) (K_D~28 nM) was added (all competition experiments were performed with standard additions of Ca^{2+}). In comparison, the number of binding complexes for labeled Srx or Srx(C99S) (B_{max}~0.31(0.31), respectively) were essentially halved in the presence of unlabeled, intact Srx or Srx(C99S) (B_{max}~0.13(0.15), respectively; Fig.6, panels A, B). Additionally, we show that labeling of S100A4 with QSY®35 does not substantially affect its binding to Srx(C99S). The “back-titration” of Alexa®546-labeled Srx(C99S), pre-incubated with 150 nM QSY®35-labeled S100A4, with unlabeled intact S100A4 almost halved its binding (Fig. 6, panels C). Intrinsic equilibrium dissociation constants calculated from “back-titrations” of labeled Srx or Srx(C99S) with intact S100A4 (K_D ~63.0 and ~33.0 nM, respectively) were similar to those for QSY35-labeled S100A4 (Table 2, experiments performed with standard additions of Ca^{2+}). While increased displacement of labeled S100A4 binding to Srx(C99S) by higher concentrations of intact protein infers some differences in binding between WT

and mutant Srx (Fig. 6, panel C), our data confirmed that the effects of fluorescent labeling on Srx(C99S)-S100A4 binding were minimal.

Srx levels influence filamentous actin structures and cell adhesion

We examined the impact of Srx expression levels on actin cytoskeletal structure/function. A549 cells with Srx expression levels at: normal (WT), depleted by shRNA (Srx KD) or over-expressing (Srx OE) were used to visualize the effect of Srx on filamentous actin and Tyr^{397}-phosphorylated focal adhesion kinase (P-FAK). Immunofluorescent staining of A549 cells showed that Srx influenced both cytoskeletal architecture and focal contacts (Fig. 7). For example, Srx OE cells exhibited more prominent stress fibers and more mature, but less numerous, focal adhesions. By contrast, control and Srx KD cells had reticular patterns of microfilaments. Srx KD cells also had more numerous, but less mature focal contacts compared to both control and Srx OE cells. Further, P-FAK staining of Srx KD cells was less on the periphery of the cells and more in the perinuclear region compared to both control and Srx OE cells.

For further investigation of the role of Srx in cell adhesion and microfilament structure, we performed adhesion assays and measured the ratio of globular to filamentous actin in cells with variable Srx levels. Confirmation that shRNA depleted Srx (essentially below detection) and that transfection increased Srx (~4-fold) levels is shown in Fig. 8A. More Srx KD cells adhered to fibronectin-coated dishes than control cells, whereas significantly fewer Srx OE cells adhered (Fig. 8B). Commensurate with adhesion, compared to WT cells, Srx KD cells had an increased ratio of P-FAK to total FAK and Srx OE cells had a decreased ratio, although this trend did not reach statistical significance (Fig. 8C). In addition, Srx OE cells had an increased ratio of globular (G) to filamentous (F) actin compared to both control and Srx KD cells (Fig. 8D). Although the decreased adhesion and filamentous actin in Srx OE cells might appear to contradict the immunofluoresence data where actin stress fibers and focal adhesions are clearly visible in Srx OE cells, it should be noted that the immunoblots of P-FAK and G and F actin permit quantification of total cellular levels of these proteins. Immunofluoresence shows large, mature focal adhesions of Srx OE cells apparently outnumbered by nascent adhesions and less mature focal contacts in the control and Srx KD cells (Fig. 7). Similarly, although Srx OE cells display prominent stress fibers that are bundles of F-actin, the control and Srx KD cells have more F-actin. Overall, these data show that Srx has a marked affect on cytoskeletal architecture and adhesion of A549 cells.

Srx levels affect cell motility

We hypothesized that the Srx-S100A4-NMIIA interaction should influence cell migration. To test this, we performed scratch assays using A549 cells with varying degrees of Srx expression. Srx over-expression resulted in a substantial increase in the rate of gap filling between “wound” edges implying enhanced planar cell motility (Fig. 9). In addition, migration by Srx knockdown cells was significantly slower than cells with WT Srx levels. For these experiments, we used two independent over-expressing or knockdown and vector only control cell lines (WT Srx) and all gave consistent results that Srx expression influences motility of A549 cells.

Discussion

Our current study identifies S100A4 and NMIIA as novel Srx binding partners. Within this context, Srx influences cell migration, adhesion and cytoskeletal architecture. Srx forms a complex with S100A4 the stability of which is enhanced by S-glutathionylation of the latter. We propose that S-glutathionylation of S100A4 increases its affinity for Ca^{2+} analogous to

results reported for S100A1 (20). Although Srx is reported to deglutathionylate actin, PTP1B and PrxI (5, 8, 9), in the present study increased Srx levels were associated with increased S100A4 S-glutathionylation while decreased Srx levels were associated with decreased S100A4 S-glutathionylation. Therefore we speculate that Srx binds to S-glutathionylated S100A4 but does not catalyze the deglutathionylation of this protein. Thus, we propose that Srx modulates S100A4 activity through an increase in Ca^{2+} binding/release and changes in specific targeting regarding NMIIA de-polymerization (Fig. 10). Cysteine residues 81 and 86 of S100A4 are implicated in S100A4 – NMIIA interactions (25), raising the possibility of redox mediated S100A4 – NMIIA interactions that may be regulated by Srx. Our proposed model of Srx promotion of S100A4 – NMIIA interaction is consistent with our observations that increased Srx expression leads to increased cell migration. The NMIIA heavy chain can be S-nitrosylated at Cys residues 90, 895 and 916 and in the presence of millimolar GSH S-nitrosylated cysteines are rapidly converted to S-glutathionylated residues (38). NMIIA may be a substrate for Srx-mediated deglutathionylation of Cys 895 or 916 and would be expected to affect monomer:dimer:multimer equilibria since these residues are located in the NMIIA heavy chain dimerization domain. Thus, given that Srx and NMIIA interactions increased following oxidative stress, Srx could promote NMIIA activity by enacting deglutathionylation; although, this possibility is not explicitly shown in the model proposed in Fig. 10. This may also explain the increased migration of Srx OE cells in wound healing assays.

Nodal linkages between redox and various aspects of cell motility, including invasion and metastasis have been reported. For example, a role for reactive oxygen species (ROS) generated by the NADPH oxidase (Nox) has been implicated in the formation and function of cancer cell invadopodia. Specifically, Tks5 facilitates the production of ROS, determined to be necessary for invadopodia formation, and in turn, ROS modulates Tks5 tyrosine phosphorylation in a positive feedback loop (39). Nox family enzymes have been linked with functional aspects of invasion and metastasis (13, 14) and enhanced generation of superoxide anion radicals by Nox may result in its spontaneous dismutation into H_2O_2 or facilitate interaction with NO [with subsequent peroxynitrite ($NOOO^-$) generation]. Subsequent cysteine nitrosylation/S-glutathionylation can influence actin-myosin interactions (16, 17, 40). The redox functions of Srx could contribute in providing homeostatic balance to the oxidative properties of the Nox system with consequent influence on cell motility and migration. High expression of Srx was shown in human solid tumors, particularly skin and lung cancers and it was found to be required for the growth, migration and invasion of human lung cancer cells *in vitro* (2). One downstream target of Srx-mediated cell signaling is PrxIV and knockdown of PrxIV mimicked the phenotypic changes of depleting Srx. Knockdown of Srx reduced anchorage independent growth in soft agar, cell migration in a wound-healing assay and cell invasiveness (41). Collectively, these data suggest that the Srx-PrxIV axis is critical in human lung cancer cell maintenance, migration and invasion. Although our present data suggest a discrepancy in that elevated Srx is linked with reduced adhesion, these general conclusions are also consistent with our findings that Srx mediates these events through a multi-protein complex that could include NMIIA and S100A4.

Unexpectedly, Srx shares quite high sequence homology with the IQGAP family of scaffolding proteins that bind to the Rho GTPases Cdc42 and Rac1 (42). BLAST (Basic Local Alignment Search Tool; http://blast.ncbi.nlm.nih.gov) analysis revealed that the entire coding sequence of hSrx1 has 86% nucleotide sequence identity with a region of the ras GTPase-activating like protein IQGAP2. At the amino acid level, an 18-residue (18–35) region of Srx has a 50% positive relationship within a region of IQGAP2 that binds Cdc42 and Rac GTPases, suggesting possible functional similarities. Since the published crystal

structure of Srx starts at amino acid residue 32 (1XW3, PDB), the structural model of Srx shown in Fig.2B excludes 14/18 residues from the homologous site and the four residues that are shown are not structured. Attempts to crystallize full-length Srx have been unsuccessful, reportedly due to the glycine-rich nature of the N-terminal region of Srx. Under physiological conditions, it is conceivable that the region of Srx with homology to IQGAP2 could form a structure enabling Cdc42/Rac GTPase binding. Moreover, since the IQGAP family members are integral to many aspects of cytoskeletal regulation (42) and tumorigenesis (43), this structural overlap with Srx may indicate some divergent evolutionary relationship worthy of further consideration.

Actin-NMIIA interactions in non-muscle cells are mediated by fully Ca^{2+}-loaded S100A4 and our results show that Ca^{2+} binding by S100A4 is influenced by its S-glutathionylation. S-glutathionylation of the Cys85 of S100A1 also causes structural modifications and enhanced Ca^{2+} binding (20). The most conserved regions within the S100 protein family are the Ca^{2+}-binding motifs, the EF-hands, which are involved in subunit dimerization conferring biological functionality (44). Ca^{2+}-loaded S100A4 binds to NMIIA via a motif at the C-terminal end of the coiled-coil region of myosin and the interaction results in a disassembly of myosin filaments (23). Its tight affinity for Ca^{2+} is increased by several orders of magnitude in the presence of NMIIA. By binding to the C-terminal EF hand of S100A4, Ca^{2+} causes a large conformational change and exposes a hydrophobic surface containing residues in the hinge region, α-helixes III and IV, and the C-terminal loop. This hydrophobic surface is part of the NMIIA recognition site stabilizing the quaternary structure of the complex (23). This is consistent with our data [increased emission of deprotonated tyrosine (tyrosinate) (37)] indicating that the tertiary and quaternary structures of S100A4 (and in particular S100A4-SSG) is influenced by Ca^{2+} (Fig. 4C). Tyr75 (α-helix IV) of S100A4 is essential for homodimerization (45). Specific to S100A4, the proximity of Cys76 to Tyr75 could be relevant to our tyrosinate fluorescence data that indicate tertiary/quaternary structural changes. Thus, Cys76 S-glutathionylation may shift S100A4 monomer-dimer equilibrium. Our present *in vitro* data support such a hypothesis, but further experiments will be required to prove that this occurs *in vivo*. Because of its tight binding to S-glutathionylated S100A4, increased levels of Srx may promote S100A4 activity towards NMIIA. Our titration data (using 0–0.5μM of S100A4 and S100A4-SSG) showed that binding to Srx and SrxC99S is specific and is enhanced by Ca^{2+} (Table 2), regardless of the fact that the interface of these proteins (aa 51–64 (α-helix III) for S100A4 and aa 130–136 for Srx) does not involve the EF motifs (Molecular modeling, Fig. 1D). An increase in the affinity of S-glutathionylated S100A4 for Srx signifies an increased stability of this complex and consequently, may result in Srx-specific targeting of NMII. The latter could affect the S100A4-Srx complex bound/free state and Ca^{2+} equilibrium for the actin/NMII interaction. Our data suggest that low affinity binding of Srx with S-glutathionylated S100A4 might occur only after saturation of the high affinity binding sites. Such high affinity binding may cause structural changes only in Srx (not Srx C99S) implying that the Cys99 in Srx is involved in heterodimerization with S100A4.

The “floodgate” hypothesis of H_2O_2 signaling considers that peroxiredoxins are inactivated by hyper-oxidation to allow local accumulation of H_2O_2 for signaling purposes (46). Thus, Srx can reactivate peroxiredoxins maintaining “physiological” H_2O_2 levels. However, hyper-oxidized peroxiredoxins are not detectable during physiological H_2O_2 signaling (47) and phosphorylation of Tyr194 of membrane associated PrxI inactivates it following growth factor stimulation during wound healing allowing a transient accumulation of H_2O_2 around membranes (48). This implies that in addition to reducing over-oxidized peroxiredoxins there may be further physiological functions for Srx. Our results define a role for Srx as a redox-regulated specific S100A4-carrier, participating in cytoskeleton remodeling functioning in cellular mobility/motility regulation. Overall, we propose the model in Fig.

10, which is consistent with the data generated. Initial S-glutathionylation of S100A4 mechanistically activates it through increasing its binding affinity for Ca^{2+}, thereby exposing internal hydrophobic areas of the monomers. Srx binds with high affinity to the S-glutathionylated and Ca^{2+}-loaded S100A4 stabilizing the active S100A4. Srx bound to S100A4 then binds to NMIIA either through (i) S100A4:NMIIA binding or (ii) Srx:NMIIA binding – in either case promoting NMIIA filament disassembly thereby affecting cell migration and adhesion. This model supports the conclusion that Srx interactions with NMIIA and S100A4 have a functional redox role in controlling cell motility, migration and adhesion.

Acknowledgments

This work was supported by grants from the National Institutes of Health (CA08660 and CA117259) support from the National Center for Research Resources (5P20RR024485- 02) and the National Institute of General Medical Sciences (8 P20 GM103542-02) and the South Carolina Centers of Excellence program. We thank the Drug Metabolism and Pharmacokinetics and Proteomics Core Facilities at the Medical University of South Carolina. This work was conducted in a facility constructed with support from the National Institutes of Health, Grant Number C06 RR015455 from the Extramural Research Facilities Program of the National Center for Research Resources.

Abbreviations

FAK	focal adhesion kinase
GSH	glutathione
KD	knockdown
NMIIA	non-muscle myosin IIA
NOS	nitric oxide synthase
NOX	NADPH oxidase
OE	over-expressing
PABA/NO	(O^2-[2,4-dinitro-5-[4-(N-methylamino) benzoyloxy] phenyl]1-(N,N-dimethylamino) diazen-1-ium-1,2-diolate)
Prx	peroxiredoxin
Srx	sulfiredoxin

References

1. Finkel T. Signal transduction by reactive oxygen species. The Journal of cell biology. 2011; 194:7–15. [PubMed: 21746850]
2. Wei Q, Jiang H, Matthews CP, Colburn NH. Sulfiredoxin is an AP-1 target gene that is required for transformation and shows elevated expression in human skin malignancies. Proc Natl Acad Sci U S A. 2008; 105:19738–19743. [PubMed: 19057013]
3. Planson AG, Palais G, Abbas K, Gerard M, Couvelard L, Delaunay A, Baulande S, Drapier JC, Toledano MB. Sulfiredoxin Protects Mice from Lipopolysaccharide-Induced Endotoxic Shock. Antioxidants & redox signaling. 2011
4. Bae SH, Sung SH, Cho EJ, Lee SK, Lee HE, Woo HA, Yu DY, Kil IS, Rhee SG. Concerted action of sulfiredoxin and peroxiredoxin I protects against alcohol-induced oxidative injury in mouse liver. Hepatology. 2011; 53:945–953. [PubMed: 21319188]
5. Park JW, Mieyal JJ, Rhee SG, Chock PB. Deglutathionylation of 2-Cys peroxiredoxin is specifically catalyzed by sulfiredoxin. J Biol Chem. 2009; 284:23364–23374. [PubMed: 19561357]

6. Woo HA, Jeong W, Chang TS, Park KJ, Park SJ, Yang JS, Rhee SG. Reduction of cysteine sulfinic acid by sulfiredoxin is specific to 2-cys peroxiredoxins. J Biol Chem. 2005; 280:3125–3128. [PubMed: 15590625]
7. Biteau B, Labarre J, Toledano MB. ATP-dependent reduction of cysteine-sulphinic acid by S. cerevisiae sulphiredoxin. Nature. 2003; 425:980–984. [PubMed: 14586471]
8. Findlay VJ, Townsend DM, Morris TE, Fraser JP, He L, Tew KD. A novel role for human sulfiredoxin in the reversal of glutathionylation. Cancer Res. 2006; 66:6800–6806. [PubMed: 16818657]
9. Lei K, Townsend DM, Tew KD. Protein cysteine sulfinic acid reductase (sulfiredoxin) as a regulator of cell proliferation and drug response. Oncogene. 2008; 27:4877–4887. [PubMed: 18454177]
10. Vicente-Manzanares M, Ma X, Adelstein RS, Horwitz AR. Non-muscle myosin II takes centre stage in cell adhesion and migration. Nat Rev Mol Cell Biol. 2009; 10:778–790. [PubMed: 19851336]
11. Garrett SC, Varney KM, Weber DJ, Bresnick AR. S100A4, a mediator of metastasis. J Biol Chem. 2006; 281:677–680. [PubMed: 16243835]
12. Parsons JT, Horwitz AR, Schwartz MA. Cell adhesion: integrating cytoskeletal dynamics and cellular tension. Nat Rev Mol Cell Biol. 2010; 11:633–643. [PubMed: 20729930]
13. Kumar B, Koul S, Khandrika L, Meacham RB, Koul HK. Oxidative stress is inherent in prostate cancer cells and is required for aggressive phenotype. Cancer Res. 2008; 68:1777–1785. [PubMed: 18339858]
14. Weaver AM. Regulation of cancer invasion by reactive oxygen species and Tks family scaffold proteins. Sci Signal. 2009; 2:pe56. [PubMed: 19755707]
15. Dalle-Donne I, Giustarini D, Rossi R, Colombo R, Milzani A. Reversible S-glutathionylation of Cys 374 regulates actin filament formation by inducing structural changes in the actin molecule. Free Radic Biol Med. 2003; 34:23–32. [PubMed: 12498976]
16. Pastore A, Tozzi G, Gaeta LM, Bertini E, Serafini V, Di Cesare S, Bonetto V, Casoni F, Carrozzo R, Federici G, Piemonte F. Actin glutathionylation increases in fibroblasts of patients with Friedreich's ataxia: a potential role in the pathogenesis of the disease. J Biol Chem. 2003; 278:42588–42595. [PubMed: 12915401]
17. Wang J, Boja ES, Tan W, Tekle E, Fales HM, English S, Mieyal JJ, Chock PB. Reversible glutathionylation regulates actin polymerization in A431 cells. J Biol Chem. 2001; 276:47763–47766. [PubMed: 11684673]
18. Tarabykina S, Griffiths TR, Tulchinsky E, Mellon JK, Bronstein IB, Kriajevska M. Metastasis-associated protein S100A4: spotlight on its role in cell migration. Curr Cancer Drug Targets. 2007; 7:217–228. [PubMed: 17504119]
19. Santamaria-Kisiel L, Rintala-Dempsey AC, Shaw GS. Calcium-dependent and -independent interactions of the S100 protein family. Biochem J. 2006; 396:201–214. [PubMed: 16683912]
20. Goch G, Vdovenko S, Kozlowska H, Bierzynski A. Affinity of S100A1 protein for calcium increases dramatically upon glutathionylation. FEBS J. 2005; 272:2557–2565. [PubMed: 15885104]
21. Lim SY, Raftery MJ, Goyette J, Geczy CL. S-glutathionylation regulates inflammatory activities of S100A9. J Biol Chem. 285:14377–14388. [PubMed: 20223829]
22. Orre LM, Pernemalm M, Lengqvist J, Lewensohn R, Lehtio J. Up-regulation, modification, and translocation of S100A6 induced by exposure to ionizing radiation revealed by proteomics profiling. Mol Cell Proteomics. 2007; 6:2122–2131. [PubMed: 17785350]
23. Badyal SK, Basran J, Bhanji N, Kim JH, Chavda AP, Jung HS, Craig R, Elliott PR, Irvine AF, Barsukov IL, Kriajevska M, Bagshaw CR. Mechanism of the Ca(2)+-dependent interaction between S100A4 and tail fragments of nonmuscle myosin heavy chain IIA. J Mol Biol. 2011; 405:1004–1026. [PubMed: 21110983]
24. Li ZH, Bresnick AR. The S100A4 metastasis factor regulates cellular motility via a direct interaction with myosin-IIA. Cancer Res. 2006; 66:5173–5180. [PubMed: 16707441]
25. Dulyaninova NG, Hite KM, Zencheck WD, Scudiero DA, Almo SC, Shoemaker RH, Bresnick AR. Cysteine 81 is critical for the interaction of S100A4 and myosin-IIA. Biochemistry. 2011; 50:7218–7227. [PubMed: 21749055]

26. Saavedra JE, Srinivasan A, Buzard GS, Davies KM, Waterhouse DJ, Inami K, Wilde TC, Citro ML, Cuellar M, Deschamps JR, Parrish D, Shami PJ, Findlay VJ, Townsend DM, Tew KD, Singh S, Jia L, Ji X, Keefer LK. PABA/NO as an anticancer lead: analogue synthesis, structure revision, solution chemistry, reactivity toward glutathione, and in vitro activity. Journal of medicinal chemistry. 2006; 49:1157–1164. [PubMed: 16451080]
27. Manevich Y, Townsend DM, Hutchens S, Tew KD. Diazeniumdiolate mediated nitrosative stress alters nitric oxide homeostasis through intracellular calcium and S-glutathionylation of nitric oxide synthetase. PLoS One. 2010; 5:e14151. [PubMed: 21152397]
28. Townsend DM, Manevich Y, He L, Xiong Y, Bowers RR Jr, Hutchens S, Tew KD. Nitrosative stress-induced s-glutathionylation of protein disulfide isomerase leads to activation of the unfolded protein response. Cancer Res. 2009; 69:7626–7634. [PubMed: 19773442]
29. Roussel X, Bechade G, Kriznik A, Van Dorsselaer A, Sanglier-Cianferani S, Branlant G, Rahuel-Clermont S. Evidence for the formation of a covalent thiosulfinate intermediate with peroxiredoxin in the catalytic mechanism of sulfiredoxin. The Journal of biological chemistry. 2008; 283:22371–22382. [PubMed: 18552404]
30. Turner J, Anderson R, Guo J, Beraud C, Fletterick R, Sakowicz R. Crystal structure of the mitotic spindle kinesin Eg5 reveals a novel conformation of the neck-linker. The Journal of biological chemistry. 2001; 276:25496–25502. [PubMed: 11328809]
31. Saijo T, Ishii G, Ochiai A, Yoh K, Goto K, Nagai K, Kato H, Nishiwaki Y, Saijo N. Eg5 expression is closely correlated with the response of advanced non-small cell lung cancer to antimitotic agents combined with platinum chemotherapy. Lung Cancer. 2006; 54:217–225. [PubMed: 16934364]
32. Dorner C, Ciossek T, Muller S, Moller PH, Ullrich A, Lammers R. Characterization of KIF1C, a new kinesin-like protein involved in vesicle transport from the Golgi apparatus to the endoplasmic reticulum. The Journal of biological chemistry. 1998; 273:20267–20275. [PubMed: 9685376]
33. Marsit CJ, Okpukpara C, Danaee H, Kelsey KT. Epigenetic silencing of the PRSS3 putative tumor suppressor gene in non-small cell lung cancer. Mol Carcinog. 2005; 44:146–150. [PubMed: 16013053]
34. Tyagi SC. Role of oxidative mixed-disulfide formation in elastase-serine proteinase inhibitor (serpin) complex. Biochem Cell Biol. 1996; 74:391–401. [PubMed: 8883845]
35. Durussel I, Blouquit Y, Middendorp S, Craescu CT, Cox JA. Cation- and peptide-binding properties of human centrin 2. FEBS Lett. 2000; 472:208–212. [PubMed: 10788612]
36. Garrett SC, Varney KM, Weber DJ, Bresnick AR. S100A4, a mediator of metastasis. The Journal of biological chemistry. 2006; 281:677–680. [PubMed: 16243835]
37. Lacowick, JR. Principles of Fluorescence Spectroscopy. Kluwer Academic/Plenum Publishers; New York: 1999. p. 450-452.
38. Greco TM, Hodara R, Parastatidis I, Heijnen HF, Dennehy MK, Liebler DC, Ischiropoulos H. Identification of S-nitrosylation motifs by site-specific mapping of the S-nitrosocysteine proteome in human vascular smooth muscle cells. Proc Natl Acad Sci U S A. 2006; 103:7420–7425. [PubMed: 16648260]
39. Diaz B, Shani G, Pass I, Anderson D, Quintavalle M, Courtneidge SA. Tks5-dependent, nox-mediated generation of reactive oxygen species is necessary for invadopodia formation. Science signaling. 2009; 2:ra53. [PubMed: 19755709]
40. Dalle-Donne I, Rossi R, Giustarini D, Colombo R, Milzani A. Actin S-glutathionylation: evidence against a thiol-disulphide exchange mechanism. Free Radic Biol Med. 2003; 35:1185–1193. [PubMed: 14607517]
41. Wei Q, Jiang Hong, Xiao Zhen, Stephen Andrew, Baker Alyson, Young Matthew R, Veenstra Timothy D, Colburn Nancy H. Srx-Prx IV axis is required for human lung cancer cell maintenance, migration, and invasion. Proc of the AACR. 2010:1481.
42. Briggs MW, Sacks DB. IQGAP proteins are integral components of cytoskeletal regulation. EMBO Rep. 2003; 4:571–574. [PubMed: 12776176]
43. White CD, Brown MD, Sacks DB. IQGAPs in cancer: a family of scaffold proteins underlying tumorigenesis. FEBS Lett. 2009; 583:1817–1824. [PubMed: 19433088]

44. Zhukova L, Zhukov I, Bal W, Wyslouch-Cieszynska A. Redox modifications of the C-terminal cysteine residue cause structural changes in S100A1 and S100B proteins. Biochim Biophys Acta. 2004; 1742:191–201. [PubMed: 15590070]

45. Tarabykina S, Scott DJ, Herzyk P, Hill TJ, Tame JR, Kriajevska M, Lafitte D, Derrick PJ, Dodson GG, Maitland NJ, Lukanidin EM, Bronstein IB. The dimerization interface of the metastasis-associated protein S100A4 (Mts1): in vivo and in vitro studies. The Journal of biological chemistry. 2001; 276:24212–24222. [PubMed: 11278510]

46. Wood ZA, Poole LB, Karplus PA. Peroxiredoxin evolution and the regulation of hydrogen peroxide signaling. Science. 2003; 300:650–653. [PubMed: 12714747]

47. Choi MH, Lee IK, Kim GW, Kim BU, Han YH, Yu DY, Park HS, Kim KY, Lee JS, Choi C, Bae YS, Lee BI, Rhee SG, Kang SW. Regulation of PDGF signalling and vascular remodelling by peroxiredoxin II. Nature. 2005; 435:347–353. [PubMed: 15902258]

48. Woo HA, Yim SH, Shin DH, Kang D, Yu DY, Rhee SG. Inactivation of peroxiredoxin I by phosphorylation allows localized H(2)O(2) accumulation for cell signaling. Cell. 2010; 140:517–528. [PubMed: 20178744]

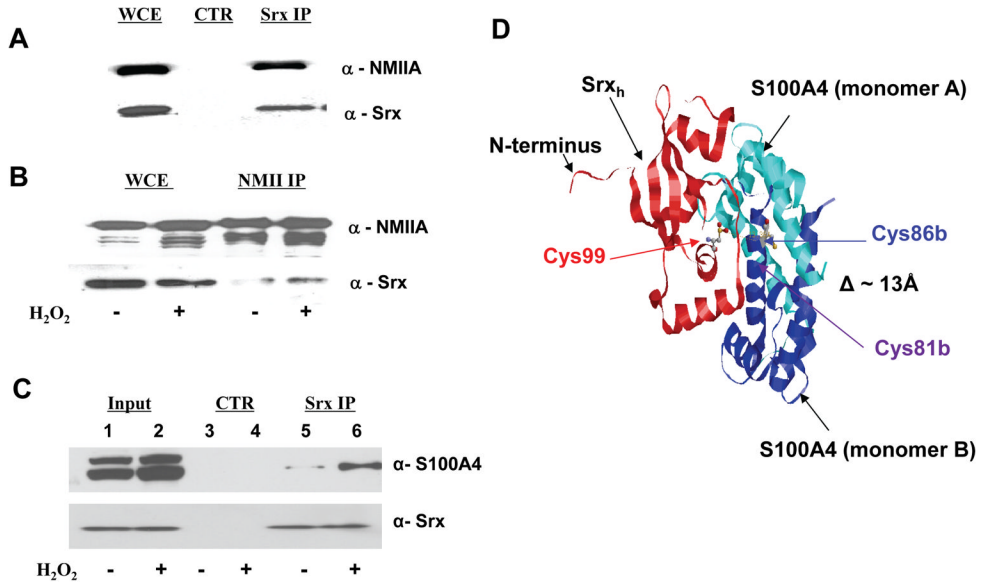

Figure 1. Srx, NMIIA and Srx, S100A4 co-immunoprecipitate in A549 cells

Panel A: FLAG-tagged Srx was immunoprecipitated from A549 cells as described in materials and methods. Whole cell extract (WCE), immunoprecipitation control (CTR) and Srx immunoprecipitates (Srx IP) were resolved by SDS-PAGE and immunoblotted with antibodies against NMIIA and Srx. **Panel B**: NMIIA was immunoprecipitated from A549 cells treated (or not) with 200μM H_2O_2 for 20 minutes and after SDS-PAGE whole cell extracts and NMIIA immunoprecipitates were immunoblotted with antibodies against NMIIA and Srx. **Panel C**: Sulfiredoxin was immunoprecipitated from A549 cells treated (or not) with 200μM H_2O_2 for 20 minutes. Whole cell extracts (input), IgG control (Control) and Srx immunoprecipitates (Srx IP) were resolved by SDS-PAGE and immunoblotted with antibodies against S100A4 or Srx. **Panel D**: Structure of S100A4:Srx complex (ZDOCK): monomers of S100A4 are in blue and light blue, and Srx is in red. Cysteine residues of both proteins are presented as “balls and sticks” using CPK color code. The complex was visualized using RasMol (v 2.7.5) software.

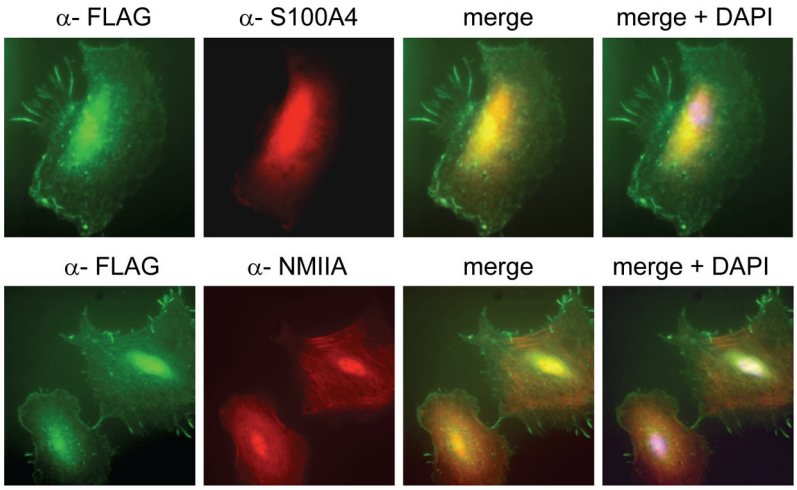

Figure 2. Immunocytochemistry reveals co-localization of Srx and S100A4 or Srx and NMIIA in A549 cells

Immunofluorescent images from A549 cells were acquired using anti-FLAG primary antibodies and FITC-conjugated secondary antibodies to detect FLAG-tagged Srx and anti-S100A4 or anti-NMIIA primary antibodies and rhodamine-conjugated secondary antibodies. Nuclei were stained with DAPI.

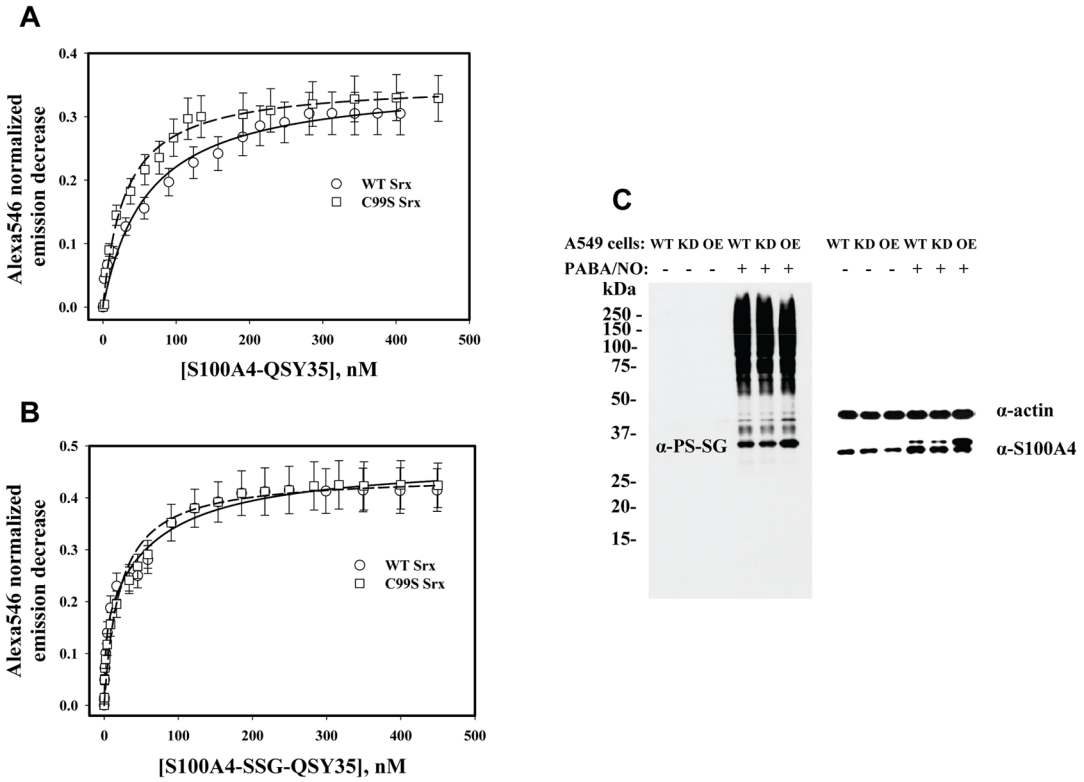

Figure 3. Effect of S-glutathionylation of S100A4 on its specific binding to Srx(C99S) *in vitro* and in A549 cells

Fluorescent analysis (for details see Materials and Methods) of S100A4-QSY®35 **(Panel A)** and S100A4-SSG-QSY®35 **(Panel B)** binding to WT(C99S) Srx-Alexa®546 [2.0 nM (Panel A) and 1 nM (Panel B)]. Solid and dashed lines represent hyperbolic fit of experimental data (for binding parameters see Table 2). **Panel C**: Effect of Srx expression levels in A549 cells on PABA/NO-induced S-glutathionylation of S100A4. Cell lysates from untreated control cells and cells treated with 20μM PABA/NO for 20 minutes were resolved by SDS-PAGE and immunoblotted with antibodies against S-glutathionylated proteins (PS-SG, left panel), or S100A4 on the same blot (right panel). Equal loading was shown by actin detection on the same blot (right panel). The upper bands migrating at ~30 kDa on the S100A4 blot superimpose with the lowest bands on the PS-SG blot suggesting that the S100A4 homo-dimer is S-glutathionylated and the increased Srx expression results in increased S-glutathionylation of S100A4 under these conditions. The blots are representative from three independent experiments.

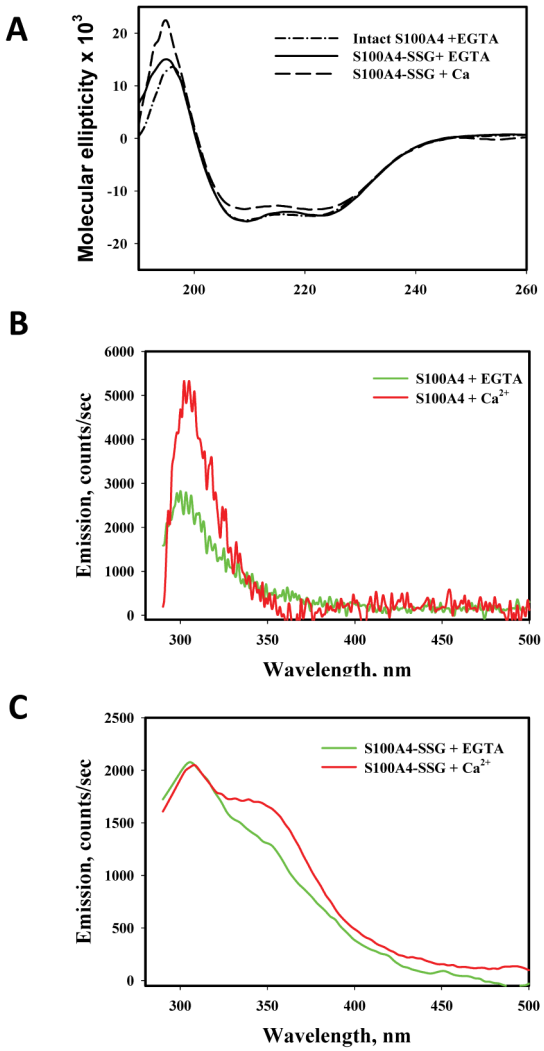

Figure 4. Recombinant human S100A4 (or S100A4-SSG) structure is influenced by Ca^{2+} and S-glutathionylation *in vitro*

Panel A: The influence of S-glutathionylation and Ca^{2+} on S100A4 protein secondary structure measured by circular dichroism. (Note that the CD spectra of S100A4 + Ca^{2+} essentially duplicated the spectrum of S100A4-SSG + Ca^{2+} and it is not presented). **Panel B/C**: effect of Ca^{2+} (100 μM, red trace) or EGTA (2mM, green trace) on tyrosine fluorescence of intact (**Panel B**) or S-glutathionylated (**Panel C**) rhS100A4. Traces on panels are representative from three independent experiments.

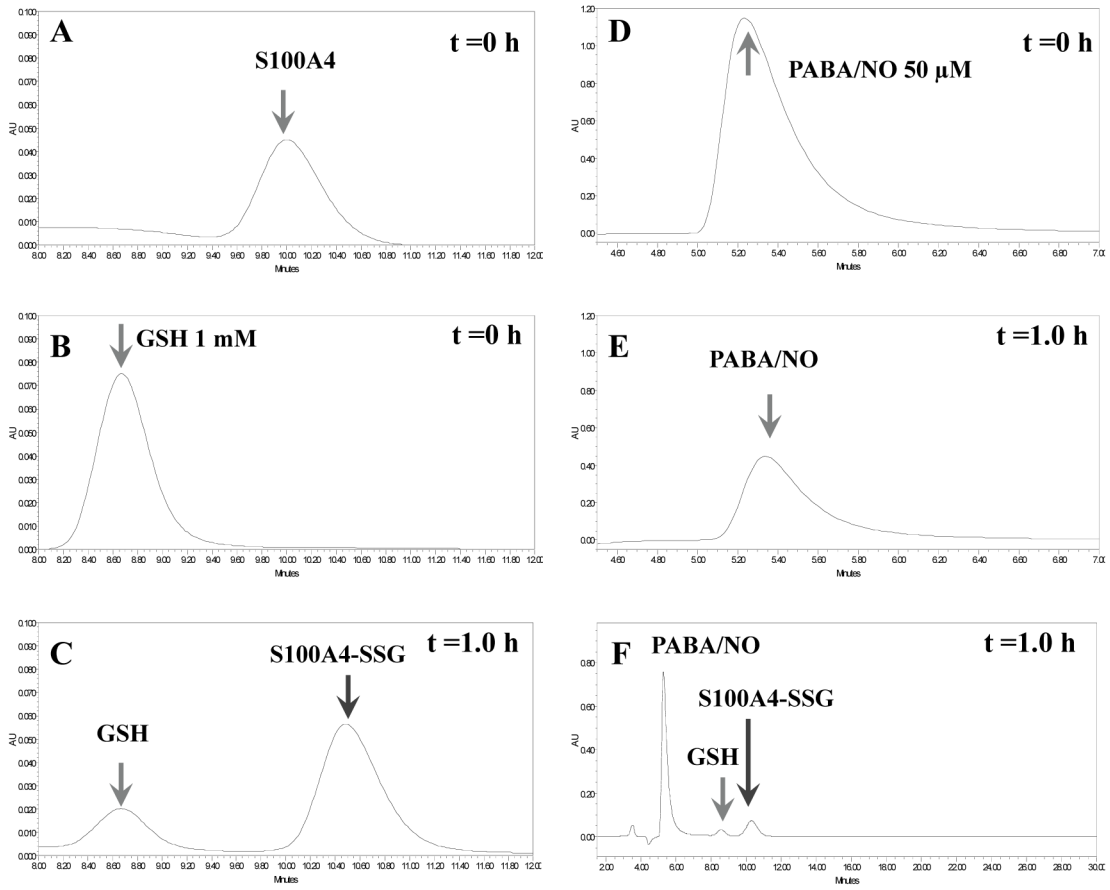

Figure 5. HPLC analyses of *in vitro* S100A4 glutathionylation by PABA/NO and GSH

Our data show completion of S100A4 S-glutathionylation (with retention time (RT) increases from 10.0 to 10.5 min) in 1 h. at room temperature. This reaction was accompanied by a decrease of the GSH peak (~80%) without changes in RT (8.65 min) as well as by a decrease of the PABA/NO peak (~62%) with subsequent increase of RT from 5.25 to 5.35 min.

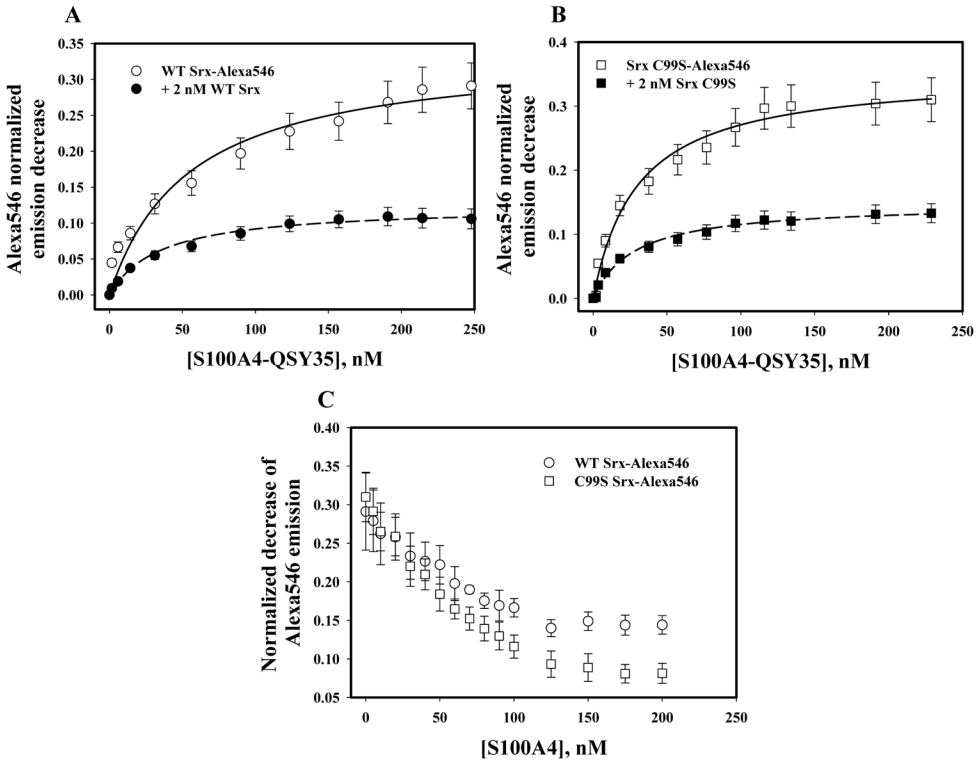

Figure 6. Effect of Srx(C99S) and S100A4 fluorescent labeling on their binding affinity

Addition of unlabeled intact Srx(C99S) proteins (both 2.0 nM) to Alexa®546-labeled Srx (**Panel A**) or C99S (**Panel B**) (both 2.0 nM) results in ~2-fold decrease in binding sites for S100A4-QSY®35 without significantly altering binding affinities. Binding isotherms representing back titrations of Srx or Srx(C99S)-Alexa®546 (both 2.0 nM, pre-incubated with 150 nM of S100A4-QSY®35) with unlabeled intact S100A4 results in competitive proportional displacement of labeled S100A4 (**Panel C**). Data are mean±SD for three independent experiments. Panels A and B: solid (WT Srx) and dashed (Srx(C99S)) lines represent hyperbolic fit (R^2=0.99) of experimental data (see Material and Methods for details).

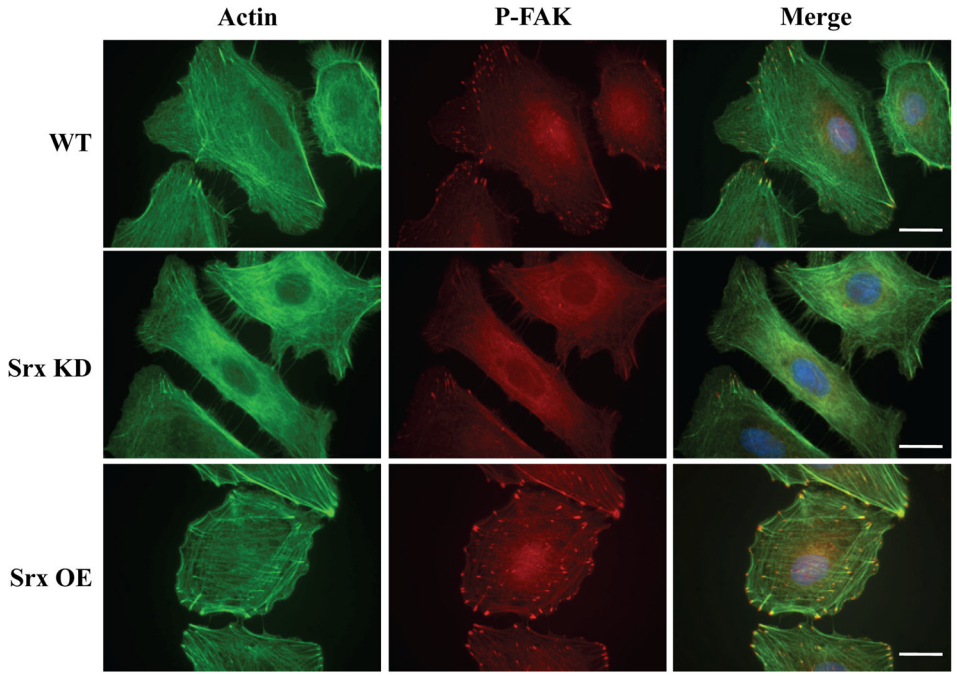

Figure 7. Sulfiredoxin expression levels affect filamentous actin and focal contacts in A549 cells

A549 cells with control Srx levels (WT Srx), Srx knockdown (Srx KD) or Srx overexpression (Srx OE) were seeded onto fibronectin-coated glass chamber slides and after 24 hrs cells that had not adhered were removed and filamentous actin and focal adhesions visualized by flourescent-labeled phalloidin and immunocytochemistry of Tyr^{397}-phosphorylated-Focal Adhesion Kinase. Bar represents 10μm.

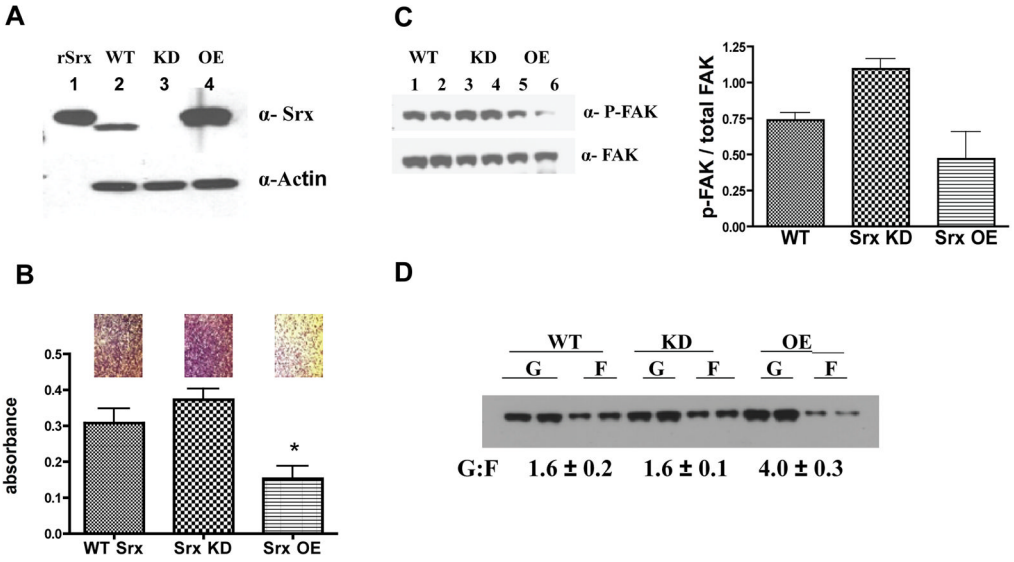

Figure 8. Sulfiredoxin affects A549 cell adhesion to fibronectin, phospho-focal adhesion kinase and filamentous actin levels in A549 cells

Panel A: Immunoblot of the cells used in panels B-D. lane 1: recombinant Srx; lane 2: A549 whole cell extract with WT Srx levels; lane 3: Srx KD; lane 4: Srx OE cells. Where relevant the actin loading control is shown below. **Panel B**: A549 cells - control (WT), shRNA-depleted (Srx KD) or Srx over-expressing (Srx OE) were plated on dishes coated with fibronectin and the number of cells that adhered after 2 hours was quantified as described in materials and methods. **Panel B insets**: Photomicrographs of crystal violet-stained A549 cells in adhesion assays. **Panel C**: Immunoblots of Tyr^{397}-phosphorylated- FAK and total FAK in A549 cells with variable levels of Srx expression after adhering to fibronectin for 24 hrs. **Panel D**: A549 cells as in Panel A were seeded onto fibronectin-coated cell culture dishes and after 24 hours cells were lysed and the ratio of globular (G) to filamentous (F) actin was quantified. The data shown are representative of three independent experiments.

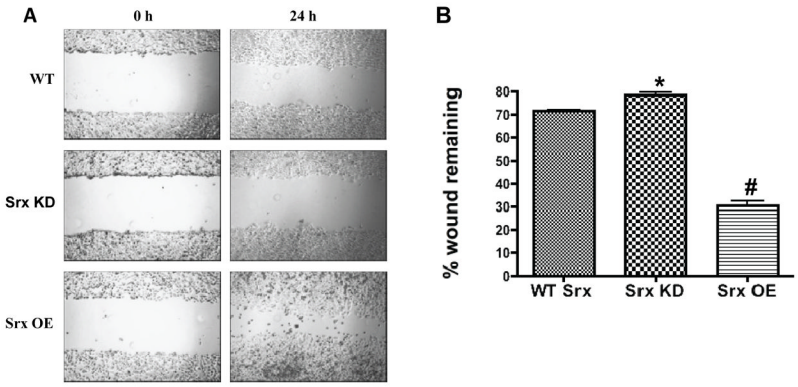

Figure 9. Over-expression of sulfiredoxin in A549 cells results in increased cell migration as determined by scratch assay

Panel A: Wild type A549 cells, A549 cells with Srx depleted by shRNA (Srx KD), and A549 cells over-expressing Srx (Srx OE) were plated in 3.5 cm dishes and allowed to reach confluence. Cell monolayers were 'wounded' with a pipette tip and photomicrographs acquired immediately afterwards and at 24 hours. **Panel B**: Quantification of three independent experiments as shown in Panel A using imageJ software. Bars with different symbols are significantly different ($P<0.05$, ANOVA) from each other.

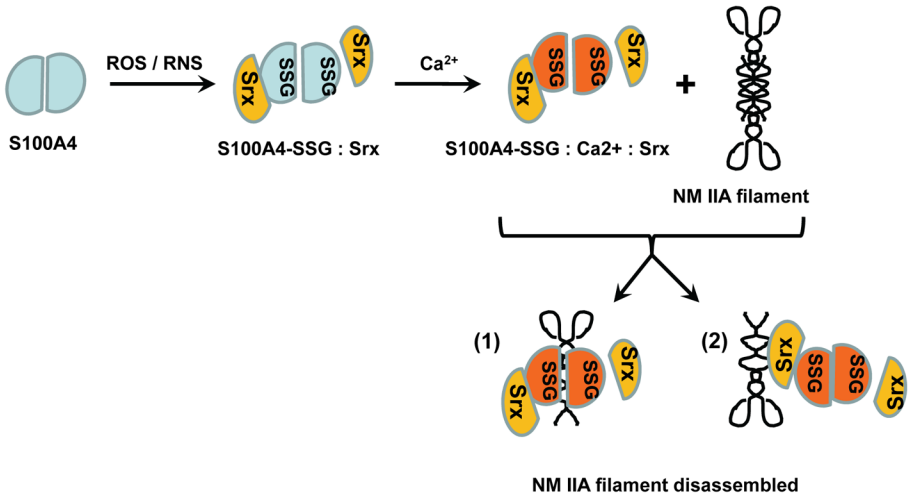

Figure 10. Model of redox-specific Srx:S100A4:NMII interactions effect on A549 cells motility/ mobility

S100A4 (light blue hemispheres) under oxidative (ROS) or nitrosative (RNS) stress conditions undergo S-glutathionylation and subsequent loading with Ca^{2+}. Srx (yellow hemispheres) binds to the S-glutathionylated and Ca^{2+}-loaded S100A4 (orange hemispheres) forming a hetero-tetramer structure. This Srx:S100A4 complex then targets NMIIA filaments either (1) through S100A4 or (2) through Srx – in either case promoting NMIIA filament disassembly and consequently promoting cell migration. For Table of Contents Use Only. Robert R. Bowers, Yefim Manevich, Danyelle M. Townsend and Kenneth D. Tew “Sulfiredoxin redox-sensitive interaction with S100A4 and non-muscle myosin IIA regulates cancer cell motility”

Table 1

MS identification of the Srx binding partners identified by co-immunoprecipitation in A549 cells.

Protein	Molecular Weight	Number of unique peptides	Protein probability	XC Score of protein	NCBI Accession number
Sulfiredoxin 1 homolog	14250.4	7	8.84E-07	80.21	22129778
Protein phosphatase 1B isoform 2	42743.8	2	7.16E-04	28.12	29558022
Peroxiredoxin III isoform b	25822.3	2	3.62E-09	20.23	32483377
Thioredoxin peroxidase (Peroxiredoxin IV)	30520.8	2	2.31E-08	20.15	5453549
Calmodulin-like 5	15882.8	2	5.21E-06	20.15	55859601
Serine protease 3 (hCG22067 or PRSS3)	29691.7	2	1.51E-04	24.11	119572363
Kinesin family member 11 (Eg5)	119084.9	5	3.74E-07	50.21	13699824
Myosin; heavy polypeptide 9, non-muscle	226390.6	7	1.07E-05	70.25	12667788

Table 2

Effect of S-glutathionylation (-SSG) and Ca^{2+} on S100A4 binding to Srx(C99S).

Srx	S100A4		S100A4-SSG	
	EGTA	**Ca^{2+}**	**EGTA**	**Ca^{2+}**
WT	K_D=83.6±10.6 nM B_{max}=0.31±0.01	K_D=60.9±8.6 nM B_{max}=0.31±0.01	K_D [1]=4.9±0.5 nM B_{max} [1]=0.18±0.02 K_D [2]=124,5±25.1 nM B_{max} [2]=0.38±0.03	K_D [1]=3.5±0.6 nM B_{max} [1]=0.17±0.03 K_D [2]=122.3±21.3 nM B_{max} [2]=0.37±0.03
C99S	K_D=42.9±3.4 nM B_{max}=0.32±0.01	K_D=30.4±2.8 nM B_{max}=0.31±0.01	K_D=24.0±2.1 nM B_{max}=0.43±0.02	K_D=21.0±3.0 nM B_{max}=0.43±0.01

For experimental details see Materials and methods. Data represent mean±SE for 3 independent experiments.